Methodology for determining the electronic thermal conductivity of metals via direct nonequilibrium *ab initio* molecular dynamics

Sheng-Ying Yue,[1] Xiaoliang Zhang,[2] Stephen Stackhouse,[3] Guangzhao Qin,[2] Edoardo Di Napoli,[1,4] and Ming Hu[1,2,*]

[1]*Aachen Institute for Advanced Study in Computational Engineering Science (AICES), RWTH Aachen University, 52062 Aachen, Germany*

[2]*Institute of Mineral Engineering, Division of Materials Science and Engineering, Faculty of Georesources and Materials Engineering, RWTH Aachen University, 52064 Aachen, Germany*

[3]*School of Earth and Environment, University of Leeds, Leeds LS2 9JT, United Kingdom*

[4]*Jülich Supercomputing Centre, Forschungszentrum Jülich and JARA-HPC, 52425 Jülich, Germany*

(Received 18 May 2016; revised manuscript received 16 July 2016; published 25 August 2016)

Many physical properties of metals can be understood in terms of the free electron model, as proven by the Wiedemann-Franz law. According to this model, electronic thermal conductivity can be inferred from the Boltzmann transport equation (BTE). However, the BTE does not perform well for some complex metals, such as Cu. Moreover, the BTE cannot clearly describe the origin of the thermal energy carried by electrons or how this energy is transported in metals. The charge distribution of conduction electrons in metals is known to reflect the electrostatic potential of the ion cores. Based on this premise, we develop a methodology for evaluating electronic thermal conductivity of metals by combining the free electron model and nonequilibrium *ab initio* molecular dynamics simulations. We confirm that the kinetic energy of thermally excited electrons originates from the energy of the spatial electrostatic potential oscillation, which is induced by the thermal motion of ion cores. This method directly predicts the electronic thermal conductivity of pure metals with a high degree of accuracy, without explicitly addressing any complicated scattering processes of free electrons. Our methodology offers a route to understand the physics of heat transfer by electrons at the atomistic level. The methodology can be further extended to the study of similar electron-involved problems in materials, such as electron-phonon coupling, which is underway currently.

DOI: 10.1103/PhysRevB.94.075149

I. INTRODUCTION

The electronic thermal conductivity (κ_{el}) is one of the most important physical properties of metals. The analytical solution of κ_{el} based on the Boltzmann transport equation (BTE) and free electron model can be expressed as [1,2]

$$\kappa_{el} = \frac{\pi^2 n k_B^2 T \tau_{el}}{3m}, \tag{1}$$

where n is the concentration of free electrons, m is the electron mass, k_B is the Boltzmann constant, T is the system temperature, and τ_{el} is the collision time of free electrons, which is mainly determined by electron-electron, electron-hole, and electron-phonon scattering. In principle, we can obtain an approximate value for τ_{el} from Matthiessen's rule. However, describing every scattering process involved in the heat transfer by electrons of solid metals is too complicated. Recently, there have been a number of studies of the κ_{el} of solid metals, based on BTE methodology [3,4]. However, it is well known that the BTE of electrons is based on a single relaxation-time approximation which may not hold true for all metals. In addition, several methods have been used to evaluate the κ_{el} of liquid-phase metals within the framework of density functional theory (DFT), such as *ab initio* molecular dynamics (AIMD), using the Kubo-Greenwood equation [5–7]. In view of this, there remains a need for an effective method to evaluate κ_{el} of solid metals.

In this paper, we develop a methodology to describe the electronic heat-transport process in solid metals without explicitly addressing detailed scattering processes. From the second law of thermodynamics, we know that heat transfer in solids is driven by the temperature gradient ∇T. It should be noted that the temperature in heat transfer describes the thermal motion of atoms, i.e., the kinetic energy of nuclei. In the meantime, the vibrations of ions can lead to spatial electrostatic potential oscillation (EPO), as can be easily deduced from the mathematical expression for the total Hamiltonian of system. It easily follows that the local variation of the electrostatic potential can induce the collective oscillations of free electrons, and those free electrons near the Fermi surface can be excited above the Fermi surface and obtain additional thermal kinetic energy with respect to 0 K. These are called thermally excited electrons. Figures 1(a) and 1(b) show two cartoons describing how the thermally excited electrons move in the vibrational lattice and the local EP field. Higher temperatures, which induce larger and faster ionic vibrations, lead to stronger EPO. Thus, the thermally excited electrons in high-temperature regions have more kinetic energy than those in low-temperature regions. Once a stable distribution of the thermal kinetic energy of thermally excited electrons is established along the direction of ∇T, then the heat flux carried by thermally excited electrons and κ_{el} can be calculated.

II. THEORY AND EVIDENCE

To confirm this conjecture and quantify κ_{el}, we performed nonequilibrium *ab initio* molecular dynamics (NEAIMD) simulations [8,9] by modifying the Vienna *Ab initio* Simulation Package (VASP) [10,11]. The atomic heat flux was realized using the Müller-Plathe algorithm [12], in which the kinetic

*hum@ghi.rwth-aachen.de

 ©2016 American Physical Society

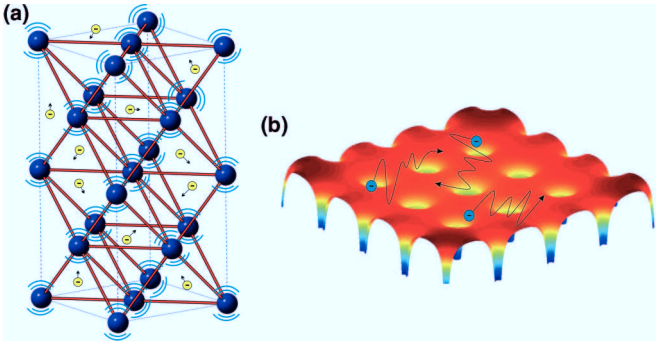

FIG. 1. Cartoons of free electrons in a metal moving in (a) the vibrating lattice and (b) electrostatic potential field.

energies of the atoms in the heat source and heat sink are exchanged (Supplemental Material [23], Sec. 1). With sufficient simulation time, we can establish a stable temperature gradient in metals. Figures 2(a) and 2(b) present the Cu model and the corresponding temperature profile, respectively. Simultaneously, we can calculate the spatial distribution and the dynamical evolution of the EP, which is expressed as

$$U = \int U(r)\rho_{\text{test}}(|r - R|)d^3r, \tag{2}$$

where the test charge ρ_{test} is the norm 1, and R represents the ion position. Figure 2(c) shows the theoretical results of the static distribution of the EP for a perfect Cu lattice. In the rest of this paper, we confirm the relationship between the spatial EPO and lattice vibrations, and that the EPO provides additional kinetic energy to thermally excited electrons. Following this, we show how to predict κ_{el} within our theoretical framework.

To demonstrate the relationship between EPO and lattice vibrations, we analyze the data from our AIMD simulations using the power spectral density (PSD) method [13,14]. For a stationary signal $x(t)$, the PSD is defined as

$$S_x(f) = \int_{-\infty}^{\infty} R_x(\tau)e^{-2\pi i f\tau}d\tau, \tag{3}$$

where $R_x(\tau) = E[x(t)x(t+\tau)]$ is the autocorrelation function of $x(t)$ [13,14], and $E[\cdots]$ denotes the expectation value. Here, we consider four signals from an AIMD simulation: atomic displacement D_{ion}, atomic velocity V_{ion}, EP displacement U_{ion}, and velocity of EPO (VEPO) ΔU_{ion}; these are used to calculate their respective spectral densities S_D, S_V [15], S_U, $S_{\Delta U}$ (Supplemental Material [23], Sec. 2). S_D and S_V reflect the frequency-dependent lattice vibrations at a specific T. Analogously, S_U and $S_{\Delta U}$ provide information regarding the EPO with respect to frequency. We show results for Al from a 10-ps equilibrium AIMD run at 100.90 K [Figs. 3(a) and 3(b)] and a 70-ps NEAIMD simulation at 299.46 K [Figs. 3(c) and 3(d)]. Figure 3(a) clearly shows that the locations of the density peaks of S_D and S_U are consistent, demonstrating that the EPO is mainly caused by the lattice vibration of ion cores. Figure 3(b) confirms this relationship. Similar results are shown in Figs. 3(c) and 3(d): for most of the frequency ranges, the peaks of S_D and S_U, S_V and $S_{\Delta U}$ are consistent with each other. However, for some specific frequencies in Figs. 3(c) and 3(d) (3.5 ∼ 5.0 THz), some

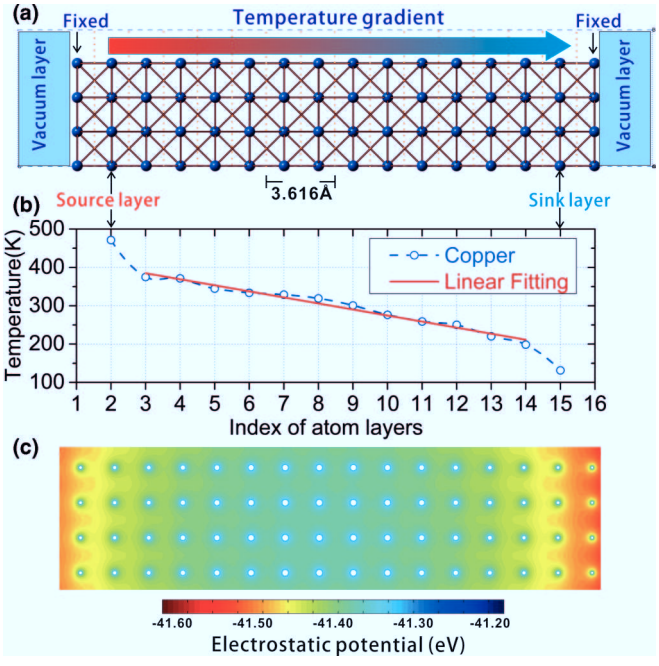

FIG. 2. Overview of the simulation model, temperature profile, and EP field of copper. (a) Model of copper used in NEAIMD simulations and (b) the corresponding temperature profile. One unit cell length comprises two layers of atoms. We use fixed boundary conditions with the layers of fixed atoms and vacuum layers along the direction of ∇T. Periodic boundary conditions are adopted in the other two dimensions. (c) Theoretical EP field of a perfect copper structure (the test charge number is norm 1).

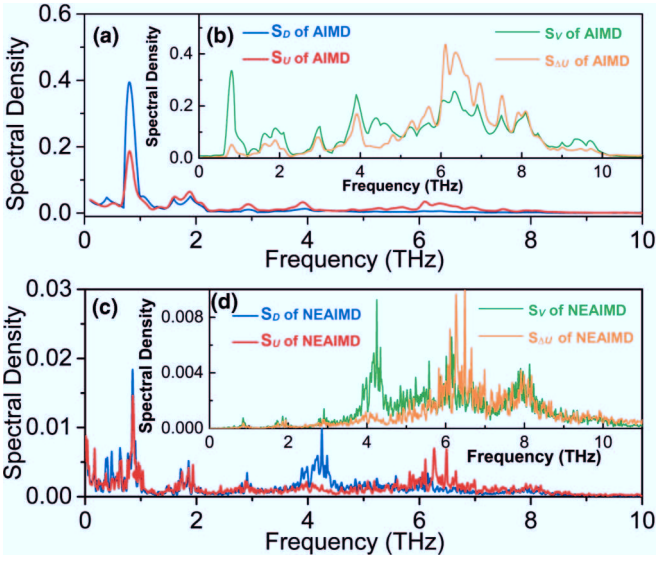

FIG. 3. Overview of the relationship between EPO at ion cores and lattice vibrations. Blue and red lines represent the spectral density of (a) atom displacements (S_D) and (c) the EP displacement (S_U), respectively, at specific ion cores. Green and orange lines represent the spectral density of (b) atom velocities (S_V) and (d) the EPO velocities ($S_{\Delta U}$), respectively, at specific ion cores. Data in (a) and (b) are from a 10-ps equilibrium AIMD simulation of Al at 100.90 K, whereas (c) and (d) present the same physical quantities from a 70-ps NEAIMD simulation of Al at 299.46 K.

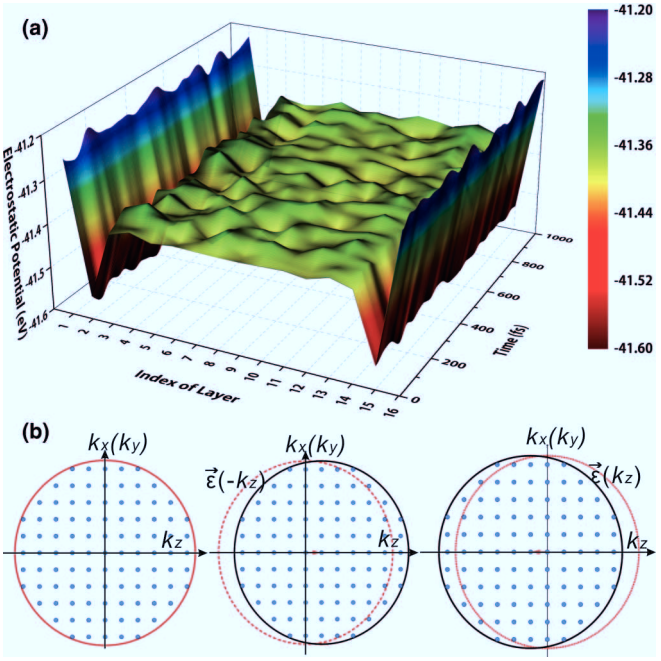

FIG. 4. (a) The variation of EPO in space over time (the test charge number is 1). Data shown are from a 20-ps NEAIMD simulation of Cu at 298.49 K. (b) Schematic of the whole Fermi sphere oscillation as local electric field vibration along the $\vec{z}$ direction.

discrepancies exist in the peaks' magnitudes. It is possible that this phenomenon could be due to the heat flux applied in the NEAIMD simulations. Nevertheless, Figs. 3(a)–3(d) provide an unambiguous physical picture of the EPO being directly induced by the lattice vibration of ions in metals.

To understand the dynamical evolution of spatial EPO intuitively, we present the representative case of Cu, calculated using NEAIMD at 298.49 K, in Fig. 4(a). Little variation occurs in the local electronic field between neighboring atom layers, and the directions of these local fields continually change with time. The variations of these local fields will drive the collective vibration of free electrons, as theoretically illustrated in Fig. 4(b). We see that only free electrons near the Fermi surface can be thermally excited. Because the direction of the local field continually changes with time, the vectors of the local momentum of the thermally excited electrons should also continually change with time. Therefore, for a sufficiently long statistical time average, no net electric current should arise during the thermal transport process of metals. This is consistent with the traditional free electron model [1].

To confirm that the EPO provides additional kinetic energy to thermally excited electrons in metals, we run a 100-ps equilibrium AIMD for Al at 329.40 K and Li at 283.97 K (both with a 2×2×2 conventional cell and 32 total atoms). When $T > 0$ K, the total energy of the free electron system can be written as [1,2] (Supplemental Material [23], Sec. 3)

$$E_{\rm sys} = E_0 + E_T = E_0 + \frac{\pi^2}{4} N \frac{(k_B T)^2}{E_F^0},$$

where E_0 is the total energy of the free electron system at 0 K, E_T is the thermally excited energy of the free electron system obtained from the outside environment when $T > 0$ K, N is the total number of free electrons, and E_F^0 is the Fermi energy at 0 K. Because the Fermi energy changes very little with temperature, here, we take the E_F at room temperature as E_F^0 and adopt the experimental data [1]. We also calculate the energy provided by EPO using

$$E_{\rm EPO} = 2\,\overline{U}_{\rm EPO}\, N\, e,$$

where $\overline{U}_{\rm EPO}$ is the average effective EPO amplitude. For Al, $E_T = 2.6293\times10^{-21}$ J and $E_{\rm EPO} = 2.7674\times10^{-21}$ J. For Li, $E_T = 1.6049\times10^{-21}$ J and $E_{\rm EPO} = 1.5909\times10^{-21}$ J. Based on these results, it is evident that

$$E_T \approx E_{\rm EPO}. \tag{4}$$

This relation, although not a strict theoretical derivation, confirms that lattice vibrations cause EPO in metals, which, in turn, induces the collective vibration of free electrons. In fact, the energy of these collective vibrations provides additional kinetic energy to the thermally excited electrons. This is the core concept underlying this methodology.

III. METHOD AND RESULTS

Within this theoretical framework, higher temperatures strengthen the spatial EPO. To confirm this relationship, we perform direct fast Fourier transform (FFT) of the relative displacement of EP $U_{\rm ion}$ and VEPO $\Delta U_{\rm ion}$. $U_{\rm ion}$ and $\Delta U_{\rm ion}$ were used to calculate S_U and $S_{\Delta U}$ in Figs. 3(a)–3(d). $U_{\rm ion}$ describes the strength of the EPO in space, whereas $\Delta U_{\rm ion}$ reflects how fast the oscillation changes. Figures 5(a) and 5(b) show the frequency-dependent FFT amplitudes of $U_{\rm ion}$ and $\Delta U_{\rm ion}$, respectively. Clearly, the EPO is stronger and faster at higher temperatures.

In Fig. 6(a), we present the positive and negative integrations of the total $\Delta U_{\rm ion}$ in the same atom layer with simulation time, which can be written as $\sum_{j=1}^{N_{al}} \sum_t \Delta U_j(t)$, where j is the index of the atom in the layer and N_{al} is the total number of atoms per layer. The four quantities in Fig. 6(a) show perfect

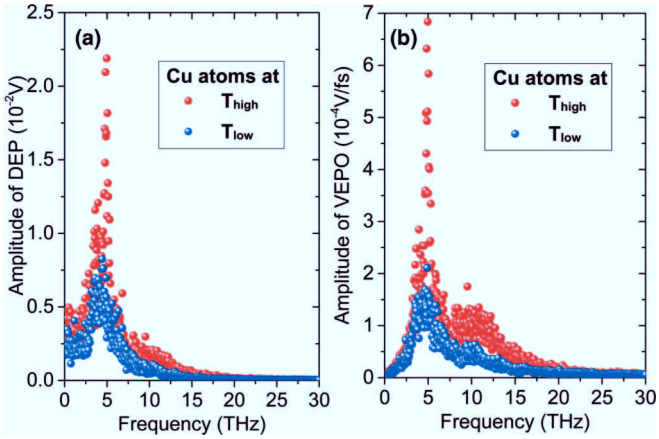

FIG. 5. The direct fast Fourier transform (FFT) amplitudes of (a) the displacement of EP (DEP, $U_{\rm ion}$) and (b) VEPO ($\Delta U_{\rm ion}$) of ion cores at different temperatures. Data shown are from a 20-ps NEAIMD simulation of Cu at 298.49 K. The high and low temperatures correspond to 374.92 K and 198.39 K, respectively.

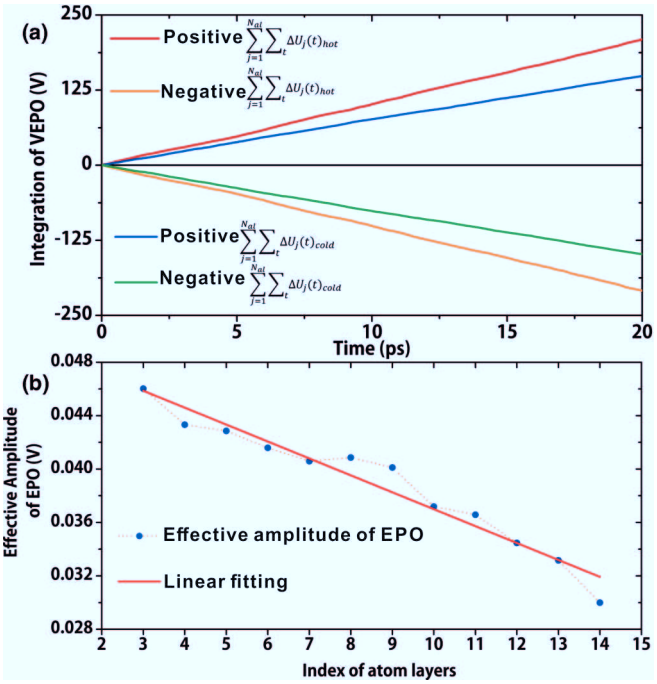

FIG. 6. (a) Integration of positive and negative VEPO $[\sum_{j=1}^{N_{al}}\sum_t \Delta U_j(t)]$ at different temperatures. (b) The effective amplitude of EPO $[\frac{1}{N_{al}}\sum_{j=1}^{N_{al}}\sqrt{\frac{1}{n_{\text{steps}}}\sum_{i=1}^{n_{\text{steps}}}(U_{ij}-\overline{U}_j)^2}$, average root mean square (rms) [16] of EPO, where N_{al} is the atom number per layer] in atom layers along the $\vec{z}$ direction. Data shown are from a 20-ps NEAIMD simulation of Cu at 298.49 K.

linear behavior over time. From the absolute values, we have

$$\sum_{j=1}^{N_{al}}\sum_t |\Delta U_j(t)_{\text{hot}}| > \sum_{j=1}^{N_{al}}\sum_t |\Delta U_j(t)_{\text{cold}}|,$$

which is consistent with the evidence shown in Figs. 5(a) and 5(b). Notably, in the same temperature region, the positive and negative accumulations of $\sum_{j=1}^{N_{al}}\Delta U_j(t)$ are almost the same. In other words, $\sum_{j=1}^{N_{al}}\sum_t \Delta U_j(t) \simeq 0$, and thus, there is no net electric field gradient along the heat flux direction for a sufficiently long statistical time. This result confirms the physical picture illustrated in Fig. 4(b). Figure 6(b) presents the distribution of the average effective amplitude of EPO in each atom layer along the heat flux direction, $\overline{U}_{\text{EPO}}(l)$, where l is the index of the atom layers. Moreover, the amplitude distribution of EPO explains how the thermal kinetic energy of thermally excited electrons is divided in space. We calculate $\overline{U}_{\text{EPO}}(l)$ using the rms method [16]:

$$\overline{U}_{\text{EPO}}(l) = \frac{1}{N_{al}}\sum_{j=1}^{N_{al}}\sqrt{\frac{1}{n_{\text{steps}}}\sum_{t_i}^{n_{\text{steps}}}[U_j(t_i)-\overline{U}_j]^2},$$

where n_{steps} is the total number of simulation time steps, $U_j(t_i)$ is the U value of atom j in a specific layer at time step t_i, and $\overline{U}_j$ is the average value of $U_j(t_i)$. Then, we define the heat flux of electrons $\vec{J}_{el}$ according to the kinetic energy of thermally excited electrons between two adjacent atom layers. Because of the isotropy of the free electron model (Supplemental Material [23], Sec. 4), we take half of the difference of the thermal kinetic energy of thermally excited electrons between the two layers as

$$\vec{J}_{el} = -\frac{1}{2}\frac{n(e)\,e}{S\,t}\frac{\partial[2\,\overline{U}_{\text{EPO}}(l)\,n_{\text{steps}}]}{\partial N_l} = -\frac{n(e)\,e\,n_{\text{steps}}}{S\,t}\frac{\partial\overline{U}_{\text{EPO}}(l)}{\partial N_l}, \quad (5)$$

where S is the cross-sectional area, t is the total simulation time, $n(e)$ is the number of free electrons per atom layer, and $\frac{\partial\overline{U}_{\text{EPO}}(l)}{\partial N_l}$ is the gradient of the average effective amplitude value of EPO by linear fitting of $\overline{U}_{\text{EPO}}(l)$ with the atom layer index number N_l shown in Fig. 6(b). Here, a nonlinear phenomenon exists in the effective EPO amplitude distribution along the heat flux direction in some metals, such as Al, Be, and Mg. According to a case study of Be, we find that the nonlinear effect of $\overline{U}_{\text{EPO}}(l)$ can be reduced by increasing the system size (Supplemental Material [23], Sec. 4.2). Because of the nonlinear effect, when we calculate the $\vec{J}_{el}$ of Al, Be, and Mg, we fit the linear part only. For Cu and Li, the $\overline{U}_{\text{EPO}}(l)$ distributions exhibit perfect linear behavior along the heat current direction. Thus, we can calculate κ_{el} based on Fourier's law:

$$\vec{J} = -\kappa\nabla T. \quad (6)$$

Combining Eqs. (5) and (6), we obtain the expression for κ_{el}:

$$\kappa_{el} = \frac{n(e)\,e\,n_{\text{steps}}}{\nabla T\,S\,t}\frac{\partial\overline{U}_{\text{EPO}}(l)}{\partial N_l}, \quad (7)$$

where ∇T is obtained by linear-fitting the temperature profile with the representative case shown in Fig. 2(b). Note that the induced temperature gradient is greater than that expected in a real system. Preliminary calculations showed that both κ_{el} and κ_{ph} were invariant to temperature gradient within the range of values studied. This can be seen in our final values for κ (Fig. 8(a); see detailed computation parameters in Table 1 and Table 3 in the Supplemental Material [23]). It should be noted that each case listed in Table 3 in the Supplemental Material [23] has a different temperature gradient, i.e., a different heat flux. In some cases the temperature gradient differs by a factor of 1.81, yet both κ_{el} and κ_{ph} show no noticeable difference. This indicates that different temperature gradients result in almost the same κ. Using larger temperature gradients (within the linear response regime) can help to establish a stable temperature profile with a smaller associated uncertainty, since the temperature difference between layers becomes greater than statistical fluctuations. It is also helpful to reduce nonlinear effects of the VEPO in space, enabling us to obtain a stable value for the thermal conductivities from both electrons and phonons. It also helps to ensure that we have enough data for statistics. As the NEAIMD is realized by the Müller-Plathe method, the temperature gradient relies on the interval time for the exchange of atomic velocities between hot and cold baths. The smaller the interval time (meaning more frequent velocity exchange), the larger the heat flux of atoms and the larger the temperature gradient. This means that with larger temperature gradients we have more valid data points to calculate the heat flux.

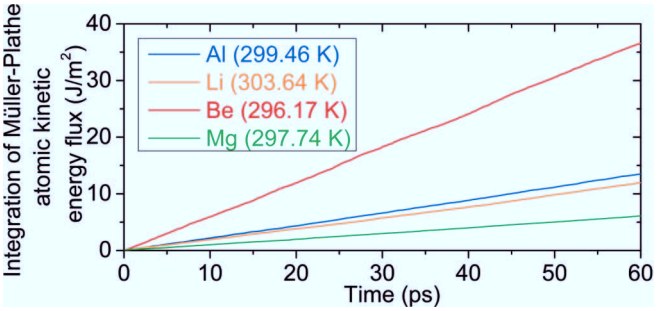

FIG. 7. Integration of the atomic kinetic energy flux with time based on the NEAIMD (Müller-Plathe) simulations of Al, Li, Be, and Mg.

Within this framework, we studied the κ_{el} of five metals (Li, Be, Mg, Al, and Cu) near room temperature. Additionally, by integrating the Müller-Plathe [12] atomic kinetic energy flux, as shown in Fig. 7, we predict the lattice (phonon) thermal conductivities of the metals (κ_{ph}). Here we adopt the statistical physics approximation that, with sufficient simulation time, the time average of κ_{el} and κ_{ph} is equal to the ensemble average. Because of finite-size effects, our NEAIMD results underestimate κ_{ph}, especially for Cu and Mg (Supplemental Material [23], Sec. 5). By summing κ_{el} and κ_{ph} from the NEAIMD simulations, we obtain the total thermal conductivities of the metals, as presented in Fig. 8(a). The results demonstrate that the thermal conductivities of metals slowly decrease with temperature near room temperature, which is consistent with traditional theory and experimental data. The error estimates

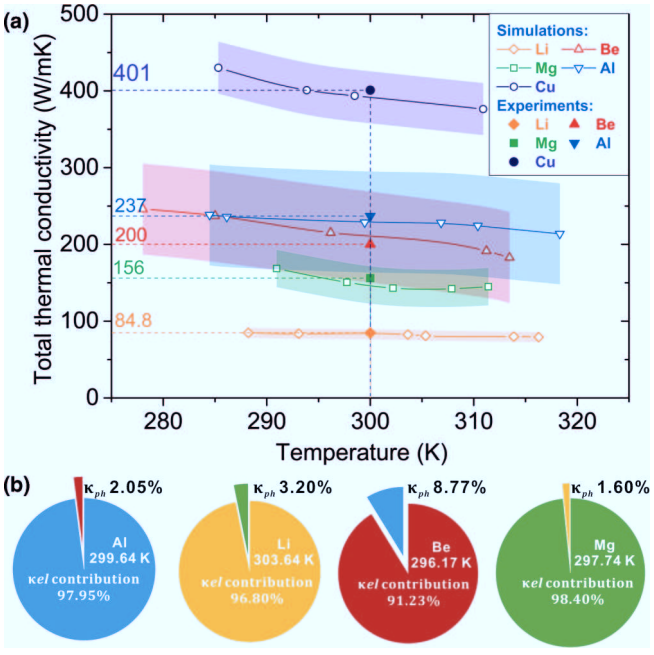

FIG. 8. NEAIMD-EPO simulation results for metals. (a) Total thermal conductivities of metals from NEAIMD simulation (with error bars determined from the calculation of ∇T and $\frac{\partial \overline{U}_{\mathrm{EPO}}(l)}{\partial N_l}$ along the heat-transport direction) and experimental data at 300 K. (b) Pie graphs showing the electronic and phononic contributions to the total thermal conductivity of Al, Li, Be, and Mg at 300 K.

in Fig. 8(a) are calculated from the expression for κ_{el} and error propagation theory [17]. They mainly stem from the calculation of the gradient of $\overline{U}_{\mathrm{EPO}}(l)$ and ∇T. Here, we note that because the statistical temperature fluctuation $\overline{(\Delta T)^2} = k_B T^2 / C_v$ [18] of each atom layer is large (because of the small number of atoms per layer), the conventional error estimate of ∇T will be quite large. However, NEAIMD consistently yields a stable temperature profile after a sufficiently long simulation time. Thus, we adopt the error in the linear fitting for ∇T. We also note that the aforementioned nonlinear phenomenon of the gradient of $\overline{U}_{\mathrm{EPO}}(l)$ can also lead to large error bars. The details of the error-bar analysis can be found in Supplemental Material [23], Sec. 6. Meanwhile, in Fig. 8(b) we use pie graphs to show the electronic and phononic contributions to the total thermal conductivity. Our results show that κ_{el} indeed dominates the thermal transport process in metals.

To the best of our knowledge, the BTE of electrons is the only theory to be relatively successful in evaluating the κ_{el} of solid metals. To compare our results with those of the traditional BTE method, we also utilize the BoltzTraP software [3] (based on electron energy band theory) to calculate $\frac{\kappa_{el}}{\tau_{el}}$. However, it is very difficult to accurately and straightforwardly calculate the lifetime of electrons. Theoretical studies indicate that the magnitude of the lifetime of electrons is around 1×10^{-14} s at room temperature [1,3,4,22], and so, similarly to previous studies [3,4], we also use the constant relaxation time approximation, with $\tau_{el} = 1\times10^{-14}$ s. To avoid finite-size effects in the calculation of κ_{ph}, we also evaluate κ_{ph} from the BTE method with interatomic force constants obtained from *ab initio* calculations [19,20], as implemented in the ShengBTE package [21]. Then, we obtain the total thermal conductivities of the metals via the BTE method by summing κ_{el} from BoltzTraP and κ_{ph} from ShengBTE. Our NEAIMD method, the traditional BTE method, and experimental data are compared in Fig. 9. The results demonstrate that the BTE method is unable to correctly describe κ_{el} for all metals, and our method is superior to the traditional BTE method in predicting the electronic thermal conductivities of metals, especially for Be and Cu at room temperature.

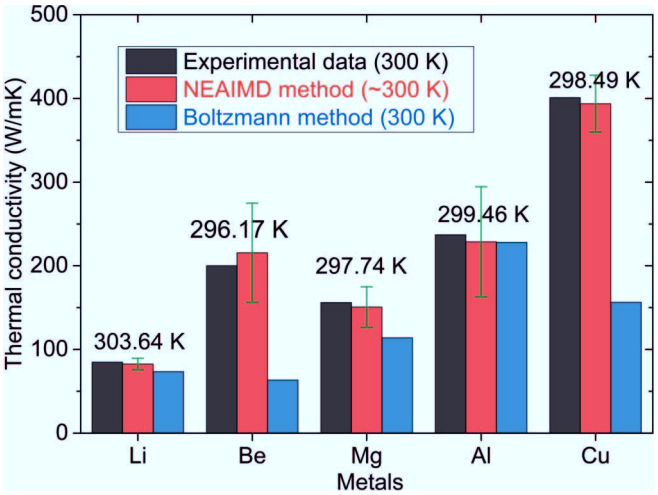

FIG. 9. Bar graph comparing the thermal conductivities of metals calculated using the NEAIMD method (with error bars), Boltzmann method, and experimental data at 300 K.

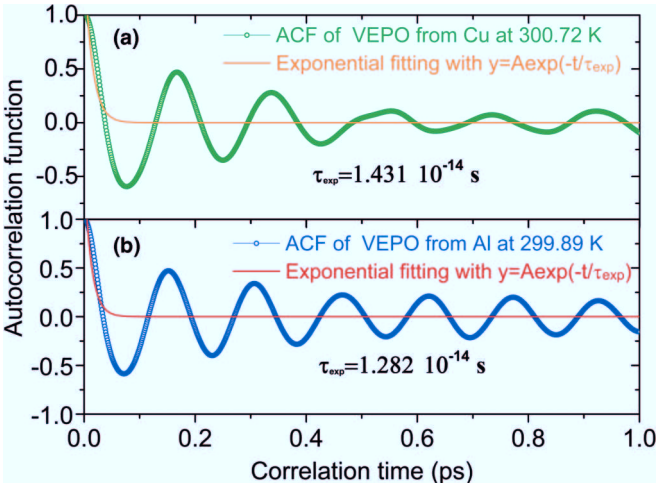

FIG. 10. Autocorrelation function of VEPO from NEAIMD simulations for the case of (a) Cu and (b) Al. The exponential fitting follows the function $y = A\exp(-t/\tau_{\rm exp})$, where $\tau_{\rm exp}$ represents the exponential autocorrelation time of VEPO.

Moreover, we observe an interesting phenomenon when calculating the spectral density of VEPO ($S_{\Delta U}$) in Figs. 3(b) and 3(d). We perform exponential decay fitting of the autocorrelation function of the VEPO using the formula $y = A\exp(-t/\tau_{\rm exp})$. Surprisingly, the exponential autocorrelation time of VEPO $\tau_{\rm exp}$ at room temperature is on the same approximate order of magnitude as the theoretical collision time of the free electrons [3,4,22]. The results for Cu and Al are shown in Fig. 10. We also examine other metals (Be, Li, and Mg) and obtain similar results (Supplemental Material [23], Sec. 8). Therefore, we anticipate that some physical mechanisms must drive this phenomenon; i.e., it is not a coincidence.

Before closing, we would like to point out that, in the BTE expression for κ_{el}, the interactions between electrons and nuclei are implicit in the electron scattering time τ_{el}, or equivalently, the presence of nuclei has a significant effect on the electron scattering time, which, in turn, affects κ_{el}. Thus, in principle, κ_{el} should depend on the vibration of nuclei. In this sense, our theory and methodology is not in conflict with the traditional free gas model. However, in contrast to the traditional electron BTE method, our direct nonequilibrium *ab initio* molecular dynamics simulation based on EPO (we name it the NEAIMD-EPO method) can calculate electronic thermal conductivity directly by mimicking the real physical picture of the heat transfer in metals, without artificial manipulation and input parameters. The NEAIMD-EPO method naturally, but implicitly, includes the complicated interactions between electrons and electron-phonon coupling. Our method is applicable to all solid metals, whereas the traditional electron BTE method struggles to evaluate κ_{el} for some elements. Our method also has some limitations, at present, such as (1) as our NEAIMD-EPO framework is built on the free electron gas model, so far, this method is limited to simulation of pure metals; (2) this method cannot be directly used to simulate thermal transport of metals at low temperatures; (3) as this method is realized in the *ab initio* molecular dynamics simulation, the simulation results will depend on the pseudopotential used; and (4) the computation costs for the NEAIMD simulations are much higher than that of normal density functional theory (DFT) simulations. However, with theory and computational capacity improving, the NEAIMD-EPO method shows potential for investigation of different kinds of electronic systems, i.e., alloys, semiconductors, metal/nonmetal interfaces, and even directly simulating nanodevices in the future.

IV. CONCLUSIONS

In summary, we have developed a methodology based on the concept of electrostatic potential oscillation to predict the electronic thermal conductivities of metals via direct nonequilibrium *ab initio* molecular dynamics simulation. We provide a clear physical picture of the origin of the thermal energy carried by electrons and reveal how this energy is transported in metals. Without explicitly addressing any complicated scattering processes of free electrons, our NEAIMD-EPO method provides better predictions of the electronic thermal conductivities of pure metals than the traditional BTE method near room temperature. Our methodology offers a route to understand the physics of heat transfer by electrons at the atomistic level. We expect that this methodology will be helpful and useful for understanding and studying the heat-transfer problems of metal systems in the future. Further extension to cope with some presently challenging problems in materials, such as electron-phonon coupling, is also foreseen.

ACKNOWLEDGMENTS

M.H. gratefully acknowledges Prof. David G. Cahill (University of Illinois at Urbana-Champaign) for valuable comments on the manuscript. S.Y.Y. gratefully thanks Dr. Yang Han (RWTH Aachen University) and Dr. Tao Ouyang (Xiangtan University) for their helpful and fruitful discussions, and Dr. Shi-Ju Ran (ICFO, Spain) for his help in plotting Figs. 1(b) and 2(c). X.Z. greatly acknowledges Dr. Zhiwei Cui (Northwestern University) for providing the input script and MEAM potential files for the EMD simulations of Li. The authors gratefully acknowledge the computing time granted by the John von Neumann Institute for Computing (NIC) and provided on the supercomputer JURECA at Jülich Supercomputing Centre (JSC) (Project ID: JHPC25). The classical NEMD and EMD simulations were performed with computing resources granted by the Jülich Aachen Research Alliance-High Performance Computing (JARA-HPC) from RWTH Aachen University under Project No. jara0135. S.S. was supported by Natural Environment Research Council (NERC) Grant No. NE/K006290/1.

[1] C. Kittel, *Introduction to Solid States Physics*, 8th ed. (John Wiley & Sons, Inc., USA, 2005), Chap. 6.

[2] W. Jones and N. H. March, *Theoretical Solid State Physics* (Courier Dover Publications, New York, 1985).

[3] G. K. H. Madsen and D. J. Singh, BoltzTraP: A code for calculating band-structure-dependent quantities, Comput. Phys. Commun. **175**, 67 (2006).
[4] M. X. Chen and R. Podloucky, Electronic thermal conductivity as derived by density function theory, Phys. Rev. B **88**, 045134 (2013).
[5] M. P. Desjarlais, J. D. Kress, and L. A. Collins, Electrical conductivity for warm, dense aluminum plasmas and liquids, Phys. Rev. E **66**, 025401(R) (2002).
[6] M. Pozzo, C. Davies, D. Gubbins, and D. Alfè, Thermal and electrical conductivity of iron at Earth's core conditions, Nature (London) **485**, 355 (2012).
[7] N. de Koker, G. Steinle-Neumann, and V. Vlček, Electrical resistivity and thermal conductivity of liquid Fe alloys at high *P* and *T*, and heat flux in Earth's core, Proc. Natl. Acad. Sci. USA **109**, 4070 (2012).
[8] S. Stackhouse, L. Stixrude, and B. B. Karki, Thermal Conductivity of Periclase (MgO) from First Principles, Phys. Rev. Lett. **104**, 208501 (2010).
[9] H. Kim, M. H. Kim, and M. Kaviany, Lattice thermal conductivity of UO_2 using *ab initio* and classical molecular dynamics, J. Appl. Phys. **115**, 123510 (2014).
[10] G. Kresse and J. Furthmüller, Efficient iterative schemes for *ab initio* total-energy calculations using a plane-wave basis set, Phys. Rev. B **54**, 11169 (1996).
[11] G. Kresse and J. Furthmüller, Efficiency of *ab initio* total energy calculations for metals and semiconductors using a plane-wave basis set, Comput. Mater. Sci. **6**, 15 (1996).
[12] F. Müller-Plathe, A simple nonequilibrium molecular dynamics method for calculating the thermal conductivity, J. Chem. Phys. **106**, 6082 (1997).
[13] W. R. Dennis, *Echo Signal Processing* (Springer, Berlin, 2003).
[14] H. V. Storch and F. W. Zwiers, *Statistical Analysis in Climate Research* (Cambridge University Press, Cambridge, UK, 2001).
[15] X. Zhang and J. Jiang, Thermal conductivity of zeolitic imidazolate framework-8: A molecular simulation study, J. Phys. Chem. C. **117**, 18441 (2013).
[16] J. R. Taylor, *An Introduction to Error Analysis: The Study of Uncertainties in Physical Measurements*, 2nd ed. (University Science Books, Sausalito, CA, 1997), Chap. 4.
[17] H. H. Ku, Notes on the use of propagation of error formulas, J. Res. Natl. Bur. Stand.: C Eng. Instrum. **70C**(4), 263 (1966).
[18] L. D. Landau and E. M. Lifshitz, *Statistical Physics*, Part 1, 3rd ed. (Pergamon Press, Oxford, UK, 1980), Chap. 2.
[19] D. A. Broido, M. Malorny, G. Birner, N. Mingo, and D. A. Stewart, Intrinsic lattice thermal conductivity of semiconductors from first principles, Appl. Phys. Lett. **91**, 231922 (2007).
[20] S. Lee, K. Esfarjani, J. Mendoza, S. Dresselhaus, and G. Chen, Lattice thermal conductivity of Bi, Sb, and Bi-Sb alloy from first principles, Phys. Rev. B **89**, 085206 (2014).
[21] W. Li, J. Carrete, N. A. Katcho, and N. Mingo, ShengBTE: A solver of the Boltzmann transport equation for phonons, Comput. Phys. Commun. **185**, 1747 (2014).
[22] I. Campillo, J. M. Pitarke, A. Rubio, E. Zarate, and P. M. Echenique, Inelastic Lifetimes of Hot Electrons in Real Metals, Phys. Rev. Lett. **83**, 2230 (1999).
[23] See Supplemental Material at http://link.aps.org/supplemental/10.1103/PhysRevB.94.075149 for information for the NEAIMD simulation step, technical information of PSD calculations and the autocorrelation function, evidence for the EPO from lattice vibrations providing the thermal kinetic energy to thermally excited electrons, details for the heat flux carried by electrons, the results and size effect of thermal conductivity (electronic and phonon) of metals from NEAIMD, analysis of error propagation, the exponential autocorrelation time of velocity of EPO at ion core, and the pros and cons of this methodology.